Review of satellite based support to forest fire environmental impact assessment: the example of Arischia (Italy) forest fire

Giovanni Laneve
University of Rome 'La Sapienza
School of Aerospace Engineering (Italy)
ORCID: 0000-0001-6108-9764
giovanni.laneve@uniroma1.it

Valerio Pampanoni
Univ. of Rome 'La Sapienza, Dep. of Astronautics,
Electric and Energetics Engineering (Italy)
ORCID: 0000-0002-9946-1303
valerio.pampanoni@uniroma1.it

Abstract

The paper aims at presenting a review of the information which satellite images can provide to support the assessment of the environmental impact of forest fires. This will be done by considering a specific fire event occurred in Italy in 2020 (L'Aquila province) which burned about 361 ha of forest. The burned area and fire damage severity has been computed by using high and very high spatial resolution satellite images and considering the maps produced by the activation of the Copernicus Emergency Management Service. The active fires have been monitored by using Low Earth Orbit and Geostationary Earth Orbit satellites. Additional information as land cover, above-ground-biomass and tree types maps, have been used to estimate burned biomass and atmosphere emissions.

Keywords: Satellite, wildfire, detection, burned area, emissions.

Resumo

Revisão do apoio por satélite à avaliação do impacto ambiental de incêndios florestais: o exemplo do incêndio florestal de Arischia (Itália). O artigo visa apresentar uma revisão do contributo das imagens de satélite no apoio à avaliação do impacte ambiental dos incêndios florestais. Esta será feito considerando um evento de incêndio específico ocorrido em Itália em 2020 (província de L'Aquila), em que arderam cerca de 361 ha de floresta. A área queimada e a gravidade dos danos causados pelo fogo tem sido calculado utilizando imagens de satélite de alta e muito alta resolução espacial e considerando os mapas produzidos pela activação do Serviço de Gestão de Emergência da Copernicus. Os fogos activos foram monitorizados através da utilização de órbita terrestre baixa e geostacionários Satélites em órbita. Informação adicional como cobertura terrestre, biomassa acima do solo e mapas dos tipos de árvore, foram utilizados para estimar a biomassa queimada e as emissões atmosféricas.

Palavras-chave: Satélite, incêndios florestais, detecção, área queimada, emissões.

DOI: https://doi.org/10.34037/978-989-9053-06-9_1.2_12

Introduction

Every year, annual reports highlight the extent of the forest fire phenomenon in the European Union, where more than half a million ha of forests burn in about 65000 fires (fig. 1) (Schmuch, 2018). This phenomenon is particularly relevant in the European Mediterranean region, where climatic factors produce a high level of vegetation stress during the summer months which causes a higher risk of inflammability.

Since the early 60s of the last century the suitability of satellite systems (NOAA/AVHRR, GOES, etc.) (e.g. by US Forest Service, (Martin, 1999)) to detect hotspots, evaluate the vegetation stress level (which can be used in the development of fire hazard maps) and estimate the burned areas has been widely recognized.

However, even if the application of earth observation satellite images dates back to almost 50 years, the evolution in the spatial resolution, spectral resolution and revisit frequency of the satellite systems allowed to improve the accuracy of the results.

For what concerns the hotspot detection techniques, the most recent algorithms using remote data are based on two or more channels (multi-channel algorithms). In particular, these algorithms use the 3.9 μm band in combination with the 10.8 μm band, which are available for the major satellite sensors used for fire detection. Remote data in these channels are often accompanied by the VIS (VISible) bands, used for the detection of pixels with cloud coverage and for the detection of false alarms.

The works of Kaufman (1998), Giglio (2016) are the most relevant for fire detection using MODIS data. For fire detection using AVHRR data, the works of Robinson (1991),

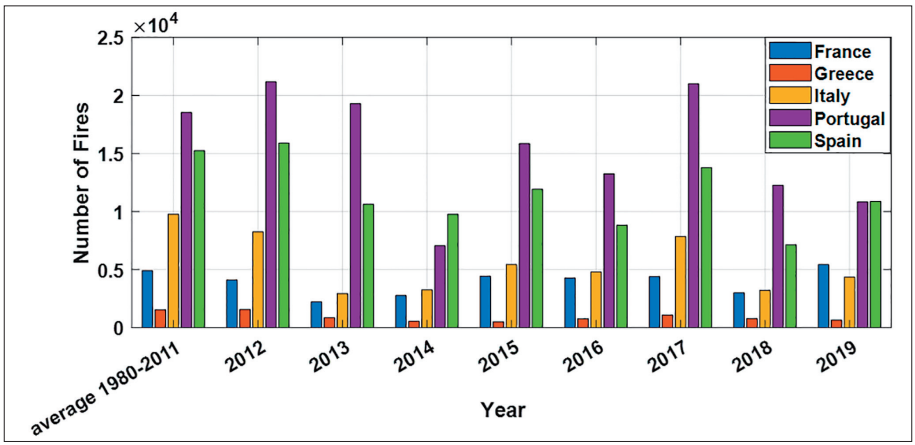

Fig. 1 - Averaged annual fire events in the European countries most affected by fires between 1980 and 2011, compared with more recent years (EFFIS-JRC annual reports).

Flasse and Ceccato (1996) are of primary importance. Concerning geostationary satellites: the works of Prins (1998) and Xu (2010) are most relevant for fire detection using the GOES (Geostationary Operational Environmental Satellite) radiometer whereas the present work is focused on the images of the MSG satellite series, operated by EUMETSAT. The SEVIRI (Spinning Enhanced Visible and Infrared Imager) sensor on board of the MSG satellite can acquire images every 15 minutes in twelve channels. These images have a 3 km resolution at the sub-satellite point (the equator), apart from the High Resolution Visible (HRV) channel (12th), which provides 1 km resolution images. For fire detection using MSG-SEVIRI data, works of Calle (2006), Laneve (2006) and Roberts *et al.* (2008) are relevant.

Mediterranean areas are at the highest risk and suffer great losses of infrastructures, forested and agricultural land, human lives and livestock. The risk of such fires is expected to increase in forthcoming years under the impact of climate changes.

Remote sensing provides a means for assessing vegetation status and monitoring changes over large geographic extents, making it a useful tool for supporting the development of fire hazard indices (Laneve, 2020). Indeed, remote sensing systems allows one to collect biophysical measurements of ground conditions before and after fire events. These measurements have been used in fire risk mapping, fuel mapping, burnt area estimates, burn severity assessing, and vegetation recovery monitoring. Therefore, in addition to the fully meteorological-based methods (Laneve, 2020), several fire hazard estimation methods based exclusively on satellite data have been proposed.

Finally, remote sensing provides a useful tool to easily and quickly detect burned areas, due to the impact that fire has on the vegetation spectral reflectances. The analysis of the changes of the post-fire signal compared with the pre-fire reflectance can provide relevant information on the impact of the fire (Chuvieco, 2019). The normalized ratio of the NIR and SWIR bands was first proposed by López García *et al.* (1991) and later named the "normalized burned ratio" (NBR). The NBR and the multitemporal versions of this index (dNBR) have been widely used in burn severity estimation. Other indices have been also proposed like the BAI (Burned Area Index) or the NDMI (Normalized Difference Moisture Index) in which the Landsat Thematic Mapper (TM) band 7 (2.09–2.35 μm) in the NBR were replaced with band 5 (1.55–1.75 μm). Other indices using the NIR and SWIR bands for burned detection are the mid-infrared burn index (MIRBI) or the modified burned area index (BAIM).

The paper is organized as follows: section 1 describes exploited data and methods; section 2 shows the results achieved by using hot spots detected on GEO and LEO orbit satellites, burned areas retrieved by using Sentinel-2 and Planet satellite images, biomass and emission in the atmosphere computed by combining satellite real-time data with ancillary maps available for the area of interest; section 3 is devoted to conclusions.

Data and Methodology

To show what is presently available in terms of information retrievable from satellite images to assess the environmental impact of forest fires, we have considered a fire event occurred in Central Italy (l'Aquila province, fig. 2) in 2020 (the fire burned from 30th of July to 13th of August). For this event an activation of the Copernicus Emergency Management Service (https://emergency.copernicus.eu/mapping/list-of-activations-rapid) was requested. Because of this activation a pre-event SPOT6 image (acquired on 06/04/2020, at a ground sampling distance of 1.5m and a post-event SPOT7 image (acquired on 04/08/2020, at a ground sampling distance of 1.5m), were acquired and used to delineate, by visual interpretation, the burned area (https://emergency.copernicus.eu/mapping/ems-product-component/EMSR449_AOI01_DEL_MONIT03_r1_RTP01/1).

To further analyze this event, we have collected the following data:

- Land cover map of the AOI (area of interest) based on Corine Land Cover 2018;
- The forest type map of the AOI based on the Copernicus Forest Type 2018 at 10m spatial resolution;
- The tree cover density map based on the Copernicus Tree Cover Density 2018 at 10m spatial resolution;
- The biomass map based on the ESA CCI (Climate Change Initiative) Biomass map at 100m spatial resolution;
- Planet satellite pre and post-event images (4 spectral channels, 4m spatial resolution);

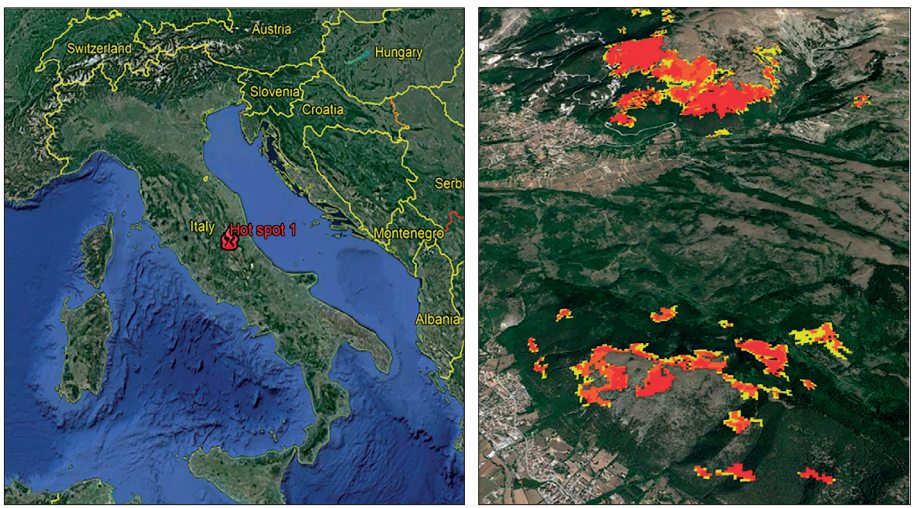

Fig. 2 - Geographic position of the area interested by the 30 July 2020 fire.

- Sentinel-2 pre and post-event images (13 spectral channels at 10, 20 and 60m spatial resolution);
- MSG/SEVIRI based hotspots computed by using the SFIDE algorithm;
- The VIIRS and MODIS sensors hotspots provided by the FIRMS website (https://firms.modaps.eosdis.nasa.gov/active_fire/#firms-shapefile);
- Vegetation type burning efficiency, smoke component emission factors taken from literature.

Methods

The burned area polygons provided by EMS activation have been assumed as a reference burned area map. Then, the burned areas have been computed using both Sentinel-2 and Planet images at a spatial resolution of 20m and 4m, respectively.

The classical method based on the computation of the NBR and RBR (Relativized Burn Ratio) (Parks, 2014) has been applied to assess the burned area using Sentinel-2. Three useful (cloud free) images of the area of interest have been found and downloaded from the Copernicus Open Access Hub. The images were acquired on 29 July 2020 (pre-event image), 3 August and 13 August 2020. The NBR has been computed on each one of the images as:

$$NBR=(NIR-SWIR)/(NIR+SWIR) \quad (1)$$

where NIR (Near InfraRed) and SWIR (Short Wave InfraRed) refer to channel 8 (0.842 μm) and 12 (2.19 μm) of Sentinel-2/MSI sensor, respectively. Then, the RBR has been computed as follows:

$$R\ BR=(NBRpre-NBRpost)/(NBRpre+1.001) \quad (2)$$

where *NBRpre* and *NBRpost* refer to the NBR values computed on the pre- and post-event images, respectively. Using this index, it is also possible to compute fire severity maps. We identify 4 thematic categories (non-burnt area, low severity, medium severity, high severity). The categorization of the level of damage is based on dNBR (difference Normalized Burn Ratio) values. This index has been extensively studied in the past, and it is computed simply as the difference between the NBRpre and the NBRpost (dNBR = NBRpre - NBRpost). Threshold values for this index have been already proposed by different researchers as well by United States Geological Survey (USGS) to

identify the different levels of damage. However, a linear correlation between dNBR and RBR can be established and used to identify the thresholds to be used to categorize the RBR maps in level of damages.

In the case of Planet images, the previous method cannot be applied since the sensor only provides a 4 spectral channel image, which lacks the SWIR channel. Therefore, in this case we used an approach based on NDVI (Normalized Difference Vegetation Index). This index is very similar to NBR with the difference that the SWIR channel is replaced by the Red channel. The detection of the burned areas is based on the computation of the dNDVI, that is the difference between NDVI values computed on the pre and post-event Planet images. Three images were used. The images, acquired on 30 July, 6 and 13 August 2020, were obtained through CUFA (Comando Unità Forestali Ambientali e Agroalimentari Carabinieri), thanks to an agreement between CUFA and University of Rome.

The MSG/SEVIRI hot spots corresponding to this event were computed by using the SFIDE algorithm developed at School of Aerospace Engineering (Faculty of Sapienza University of Rome), more details on this algorithm are given in (Laneve, 2018). The SEVIRI images are directly acquired at the University of Rome premises through the EUMETCAST service.

Hotspots detected are characterized in terms of dimensions (fire size in each pixel, p, and , where A_{PIXEL} is the area of a pixel [m^2]), fire temperature (T_f), FRP (Fire Radiative Power) and confidence level of the detection. FRP and its integration over time, FRE (Fire Radiative Energy), are further characterizations to estimate burned biomass of the pixel. Methods to compute FRP from MODIS and SEVIRI sensors are described in (Giglio, 2006), (Wooster, 2005), (Laneve, 2018).

After estimating FRP, it is possible to evaluate FRE by integrating FRP over time:

$$FRE = \int_{t_{fire}} FRP \cdot d\,t \tag{3}$$

where t_{fire} is the fire duration.

The hotspots based on LEO (Low Earth Orbit) satellites (Terra, Aqua, NPP, NOAA-20) were taken from the FIRMS website. In the case of LEO orbit satellite, in which each satellite is providing 2 images per day of the same area, the following approach, suggested in (Boschetti, 2009), has been applied:

$$\boldsymbol{F}RE = \sum_{i=1}^{N}(FRP_{t_{i+1}} + FRP_{t_i}) \cdot (t_{i+1} - t_i)/2 \tag{4}$$

where

$$FRP_t = \sum_{p=1}^{M} FRP_p \tag{5}$$

where FRP_p is the FRP retrieved by one of pixels corresponding to the active fire under analysis, M represents the number of the (thermally) anomalous pixels observed simultaneously on the burning area. Therefore, FRP_t is the sum of the FRP values retrieved at the time *t*, during the LEO satellite overpass, from all the pixels corresponding to the same fire. M represents the number of satellite overpasses during the fire event (that is, in our case, from the 30th of July to 13th of August). t_{i+1}-t_i is the time difference among two consecutive overpasses of the area.

The estimation of burned biomass (BB) can be obtained by using the following equation (Roberts, 2008):

$$BB \cong C_r \cdot FRE \tag{6}$$

where C_r is a conversion factor that links the FRP to combustion rate. In Wooster *et al.* (2005) an universal value of [kg/MJ] is proposed, while Kaiser *et al.* (2012) proposed specific values for different land cover classes. Combusted biomass density (p_B) is:

$$\rho_B \cong \frac{BB}{A_f} \tag{7}$$

Further, it is possible to estimate the emission in atmosphere by using the emission factors k_i provided for different smoke constituents and different land cover types. The emission factors for the most important smoke constituents, for different land cover classes, are provided in literature (Table I). The emission in atmosphere will be carried out by using the following relationship:

$$f(x) = \sum_{i=1}^{N} k(x)_i \cdot BB_i \tag{8}$$

where $k(x)_i$ is the emission factor of the x-th smoke component for the generic i-th land cover class and BB_i represents the burned biomass of the i-th land cover class. On the other side, if we know the biomass loading per ha, the forest type, the combustion factor for each vegetation type, and the burned area we can estimate the total burned biomass (BBtot) using the following relationship (Yi, 2016):

$$BB_{tot} = \sum_{i=1}^{N} BB_i \ \ where\ BB_i = BA_i \cdot BD_i \cdot BE_i \tag{9}$$

where *BA* (ha) is the burned area corresponding to the i-th land cover class, *BD* (ton/ha) is the dry biomass density and *BE* (%) is the burn efficiency, which is the percentage of biomass consumed by the fire.

Table I - Averaged emission factors (kg/Ton) and burning efficiency for averaged fire combustion phase for particulate matter (PM2.5), carbon dioxide (CO_2), carbon monoxide (CO), methane (CH_4).

Smoke constituents [Kg/Ton]	CO_2	CO	CH_4	PM2.5	Burning Efficiency [%]
coniferous	1617.78	97.83	4.59	12.00	40
broadleaved	1591.67	96.75	4.55	10.34	40
shrubland	1639.33	83.06	3.45	9.34	50
grassland	1606.25	62.61	2.42	8.66	90

Source: Prichard, 2020 and Li, 2017.

Results

Let us start from the assessment of the burned area. The reference burned area (provided by EMS) has been compared with the one obtained through the Sentinel-2 and the Planet images (fig. 3). The fire we analyzed, called Arischia fire, comprises two main areas (fig. 2 and fig. 3). The fire started on 30 July 2020 and ended on 13 August 2020. The burned area provided by EMS seems to overestimate the actual effect of the fire. Also, it was analyzed the details in term of the total area affected and the distribution of the level of damage as computed by using the values of RBR (Sentinel-2) and dNDVI (Planet) (Table II).

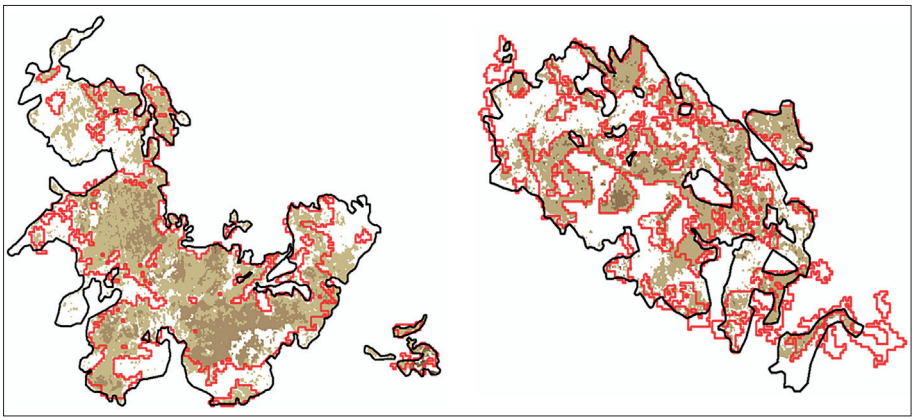

Fig. 3 - Comparison between the polygons provided by EMS (black polygons) and those obtained from Sentinel-2 images (red polygons) with superimposed burnt pixels provided by the analysis of the Planet images.

Table II - Distribution of the burned area between the different levels of damage. The estimate of the damage level is based on thresholds for dNBR available in literature.

Characteristics of the detected burned area	Copern. EMS	SIA/Planet	SIA/Sentinel-2
Total burnt area [ha]	640.0	467.0	361.0
Not burned	---	0.0	0.0
Low severity	---	142.0 (30.3%)	70.0 (20.5%)
Medium severity	---	110.4 (23.6%)	98.0 (28.4%)
High severity	---	115.0 (24.6%)	79.0 (22.4%)
Very High severity	---	100.6 (21.5%)	98.0 (28.4%)

Source: Key, 2006.

As shown by the table, automatic procedures based on the differences of the indices (NBR and NDVI) computed on pre and post-event images give remarkably different results from the ones provided by EMS. In both cases the land cover map and the tree cover density maps were considered and the analysis was carried out only on areas corresponding to the following CORINE classes: 311-Broad-leaved forest, 312-Coniferous forest, 313-Mixed forest, 324-Transitional woodland-shrub. Further, in correspondence of these classes the tree cover density should be higher than 20%. This could explain the difference between EMS and our results based on Sentinel-2 and Planet images. In fact, 30% of the area delineated by EMS corresponds to not forested areas (grassland, sparse vegetation) and area with less than 20% of tree cover density.

For what concerns the difference between Planet and Sentinel-2, this is, in our opinion, mostly related to the fact that Planet constellation images are acquired at a different local time. Therefore, the change of the shadow in such a mountainous area, can significantly affect the results. Further, the thresholds adopted to identify an area as burned and the level of severity as well, were defined through a linear relationship between dNDVI and RBR, and this is quite an important approximation since the reflectance of the vegetation in the spectral regions on which the two indices rely are differently affected by fire. However, we can estimate the level of damage through the values of the change in the indices caused by the fire. This can help to guide the recovery phase and, as we will see, the estimate of the burned biomass and emission in the atmosphere.

Concerning the active fire detection, the activation of the EMS occurred at 12:00 (UTC) of the 30 of July 2020. SFIDE algorithm (using MSG-RSS images, the MSG satellite providing images at 5min frequency) detected the first thermal anomaly at 11:30

(UTC) whereas, the first detection by FIRMS occurred at 12:00. The last detection occurred at 10:50 of 13 August and 3:42 of 14 August, respectively. However, judging by the number and distribution of hotspots (see fig. 4), the acute phase of the emergency occurred in the days between 30 July and 4 August 2020.

Both systems provide FRP computed as described in previous paragraph. Fig. 4 (left) shows the distribution of the hot spots on the reference burned area. The hot spots are given in different colors based on the time difference (in days and fractions of a day) compared to the date of the EMS activation (30 July 2020 at 14:00, Local Time). The colors range from dark red, corresponding to a detection date close to the EMS activation (July 30, 12:00, UTC), to green corresponding to the date of the last detection which took place on August 14 at 3:42 AM (local time). The different colors allow us to quickly understand where the fire started and how it spread. Fig. 4 (right) shows the same distribution of hot spots but this time the size of the circles is proportional to the intensity of the events detected. As said before, the intensity of the fire is estimated through the radiative power of the fire (FRP). This quantity, expressed in MWatts, gives a measure of the amount of the radiation emitted by the fire and therefore of the intensity of said fire. In this way it is possible, visually, to have an idea of the areas where, by type of vegetation or difficulty in the extinguishing operations, the fire has burned with greater virulence.

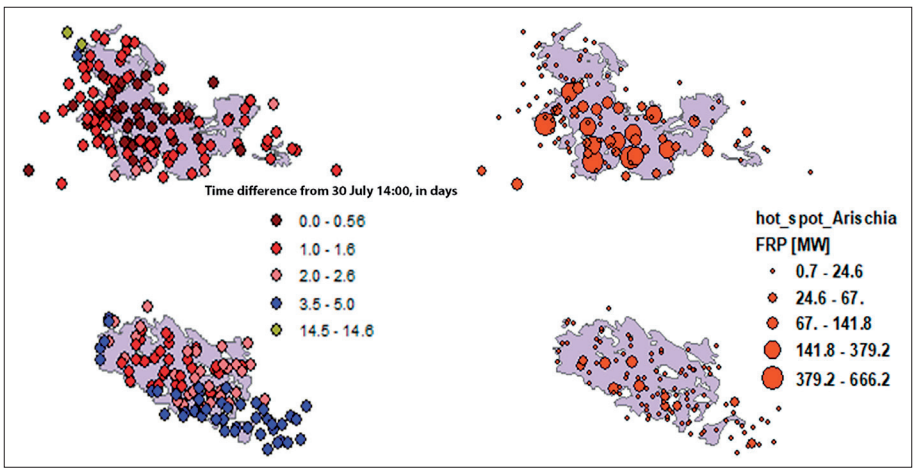

Fig. 4 – Distribution of thermal anomalies detected by the polar satellites Terra, Aqua and NPP. Different colors allow to distinguish the hotspots based on the date on which they were detected compared to the date of the EMS activation (30 July 2020 at 12:00) (Left:);
Ddistribution of thermal anomalies detected by the polar satellites Terra, Aqua and NPP. The size of the circles is proportional to the radiative power of the fire (FRP) expressed in MW (Right).

The thermal anomaly due to fires involves several MSG pixels (fig. 5). The yellow boxes of fig. 5 have a side of 2 km, corresponding, more or less, to the size of a MSG pixel at our latitude (4 km).

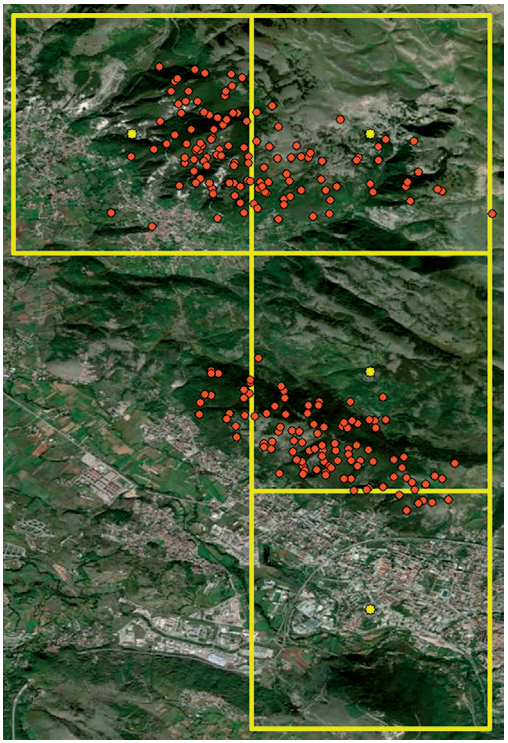

Fig. 5 – Representation of the four pixels identified in the SEVIRI/MSG image superimposed to the points (orange circles) identified by the polar orbit satellite described above. The yellow squares give an idea of the size of the MSG pixel.

The Arischia fire was also analyzed using the thermal anomalies detected by the SFIDE (System for FIre Detection) software using the images of the SEVIRI sensor on board the geostationary satellites of the MSG RSS (Rapid Scanning System) satellite which provides an image every 5 minutes. Therefore, this type of images allows an almost continuous monitoring of the fire by providing an estimate of the trend of the virulence of the event through the FRP values. In fig. 5, the orange dots represent the hotspots identified by the polar orbit satellites we talked about earlier. For each of the pixels, the FRP values are measured at a frequency of 5 minutes (fig. 6). The first detection occurred at 11:30 on 30 July 2020, half an hour before EMS activation, and the last on 13 August at 10:50.

The FRP gives the trend of the fire from the time of the first detection at 13:30, occurred in the pixels 2 and 3 in fig. 5, until the last observation of a thermal anomaly detected on 13 August at 10:50 in pixel 1 (fig. 6). The trend over time has been divided

into 2 graphs, to better appreciate the temporal variation of the FRP. As you can see, these data allow one to follow the evolution of the fire over time by providing useful information for verifying the progress of the extinguishing activity. The bottom graph of fig. 6 gives the sequence of all hot spots detected during the first 2 days of the Arischia fire. Now, combining this information with other data listed previously we can proceed with the assessment of the burned biomass and the estimate of the emission in the atmosphere.

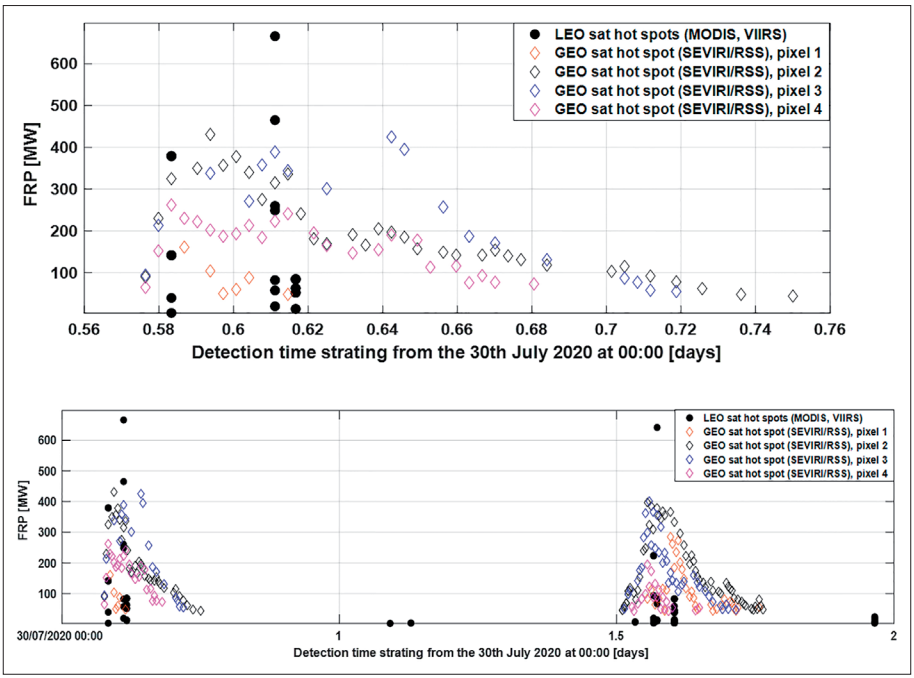

Fig. 6 - Behaviour of the Fire Radiative Power (FRP) in the four pixels corresponding to the Arischia fire for which the thermal anomaly lasted longer. The FRP corresponding to the LEO orbit satellites (black circles) are also shown in comparison. The plot on the bottom gives the FRP in logarithmic scale, so it is possible appreciate the higher sensitivity of LEO satellite sensors.

The burnt biomass can be estimated starting from the burned area delineated by using satellite images, the above ground biomass density map, the land cover map and the burning efficiency known for each vegetation type (Table I). Another way to estimate burnt biomass consists in using the radiative energy emitted by the fire and retrieved by using satellite MIR and TIR images.

The results obtained by applying the relationship given above allows us to conclude that (Table III):

- The burnt biomass estimate based on information provided by EMS appears significantly higher due to the overestimation of the burned area and the lack of any fire severity information which could allow to better evaluate the effect of the fire;
- The burnt biomass estimate based on the automatic detection of burned area by using Sentinel-2 and Planet images are quite similar to each other and amount to almost half of the value obtained using FRP;
- The burnt biomass estimate based on FRE computed by using eq. 6 and 7 through FRP retrieved by LEO orbit satellites results very similar to the one computed by using the Sentinel-2 and Planet burned area. It should be underlined that the eq.s 6 and 7 were applied, indistinctly, to all hot spots provided by FIRM. Further, a threshold of 12 hours was introduced on the time difference (t_{i+1}-t_i). That is to say, if the time difference between two consecutive overpasses is higher, the term is neglected in the sum. Since the procedure has been applied to a single case, we do not have enough data to reach any conclusion on the accuracy of this approach. We must recall that one of the limits of this method consists in the hypothesis about the burning coefficient, that is set to the constant value of 0.368 Kg/MJ;
- The burnt biomass estimate based on FRE computed trough the FRP retrieved from GEO satellites is quite lower than the one computed using LEO satellite. This is consistent with significant underestimation of the FRP typically provided by GEO satellite sensors (Li, 2017).

Table III - Burnt biomass estimated by using satellite based information: burnt areas and FRP.

	EMS burnt area	Sentinel-2	Planet	FRP/MSG	FRP/LEO
Total burnt biomass [ton]	125,003.0	16,783.0	17982.1	11417.6	16,751.1

Table IV - Fire related smoke constituents.

Smoke constituents [ton]	EMS burnt area	Sentinel-2	Planet	FRP/MSG	FRP/LEO
CO_2	202,140.0	23329.0	25598.0	18469.1	27096.6
CO	10,687.0	1315.8	1461.7	946.0	1387.9
CH_4	470.7	59.60	66.6	41.0	60.2
PM2.5	1271.6	154.2	172.0	113.2	166.1

Now we can proceed with the estimate of the emission in atmosphere by using the emission factors given in TABLE I. Taking into account land cover map, biomass density map and burned areas we can compute the fire related emissions in the atmosphere (Table IV). To retrieve the emission in atmosphere by using the burned biomass estimate obtained from FRE, we take an averaged value for the emission factors of the different smoke constituents. The averaging can be done by weighting the emission factors according to the vegetation characteristics of the burned area.

The comments already provided for burnt biomass can be repeated here, since the emission in the atmosphere depends on the burnt area, the type of vegetation involved and the fire severity. The fire regime (flaming or smoldering) is also important. The fire regime can be, in principle, assessed by using the two-channel approach (at 3.9 μm and 10.8 μm), based on the estimation of the radiant components of the pixel in absence of fire. Anyway, this information has not been considered in the computation of Table IV.

Discussion and Conclusion

This paper is devoted to review, through a practical example, which kind of information can be obtained from earth observation satellite images to support the assessment of the environmental impact of forest fires. The results shown in the paper are based on different kinds of information, not all of which are obtained from satellite images. In particular, the emission factors for different smoke components and burning efficiency, the relationship between remotely sensed fire severity and post-event vegetation conditions are taken from ground experiments. On the other hand, satellite images are used to build land cover maps, biomass density maps, forest type maps, burned area maps, hot spot maps. Satellite data can also be used to develop fire hazard maps, but even though this has been mentioned, this kind of information was not used in this paper.

The results refer to the specific fire event occurred in Italy on the 30 of July 2020 (the fire lasted 14 days, even if the more significant damages occurred from 30th July to 4th August 2020) in the Italian province of l'Aquila (Arischia municipality).

Table II, III and IV show the results in terms of burnt areas, burned biomass and emission in the atmosphere. According to the LEO satellite hotspots distribution (fig. 3 and 6), the land cover map and the forest type map, the burnt area polygons delineated by EMS (by hand, as specified in the associated report) seem to overestimate the actual extent of the area affected by the fire. As a consequence, the estimate of the burned

biomass and emission in the atmosphere is significantly higher than those computed by using the other methods described above. Indeed, the burned area estimate is 37% higher than the one computed by using dNDVI on Planet and 100% higher than the one based on Sentinel-2 images.

It is worthwhile to note that the burnt biomass estimate made by using burnt area and fire severity based on dNBR (dNDVI) and other relevant information (land cover map, biomass density, burning efficiency) are quite close to the estimate based on hotspots and FRP. The lower value provided by MSG-based hotspot was explained as due to the well-known tendency to underestimate the FRP associated to MSG images. We must underline here that, in the SFIDE algorithm, in order to minimize the number of potential false alarms, the minimum FRP threshold to consider a pixel as containing a fire has been set to 40 MW.

In conclusion, the results shown for one of the most relevant fire events that occurred in Italy in 2020, aim at demonstrating the type of information that can be retrieved from satellite images, and their strengths and limitations. EO satellite images allow to estimate burned areas and fire severity automatically and easily even if the characteristics of the sensor should be considered (in order to select the right multi-temporal index) as well as unwanted effects due to clouds or shadows. Thermal anomalies detected by using MIR and TIR channels allow to track the fire behavior (through GEO sensors) and its spread on the ground (exploiting LEO sensors). Using this information, it is also possible to assess the burned biomass and the emission in the atmosphere of GHG (Green House Gas) or other dangerous smoke constituents (PM2.5, CO).

Bibliographic references

Boschetti, L., Roy, D. (2009). Strategies for the fusion of satellite fire radiative power with burned area data for fire radiative energy derivation, *Journal of Geophysical Research*, 114, D20302.

Calle, A., Casanova, J. L., Romo, A. (2006). Fire detection and monitoring using MSG Spinning Enhanced Visible and Infrared Imager (SEVIRI) data. *Journal of Geophysical Research: Biogeosciences*, 111(G4).

Chuvieco, E., Mouillot, F., van der Werf, G. R., San Miguel, J., Tanase, M., Koutsias, N., ... & Giglio, L. (2019). Historical background and current developments for mapping burned area from satellite Earth observation. *Remote Sensing of Environment*, 225, 45-64.

Flasse, S. P., Ceccato, P. (1996) A contextual algorithm for AVHRR fire detection. *International Journal of Remote Sensing*, 17(2), 419-424.

Giglio, L., Schroeder, W., Justice, C. O. (2016). The collection 6 MODIS active fire detection algorithm and fire products. *Remote Sensing of Environment*, 178, 31-41.

Kaiser, J. W., Heil, A., Andreae, M. O., Benedetti, A., Chubarova, N., Jones, L., Morcrette, J.J., Razinger, M., Schultz, M. G., Suttie, M., van der Werf, G. R. (2012). Biomass burning emissions estimated with a global fire assimilation system based on observed fire radiative power. *Biogeosciences*, 9, 527-554.

Kaufman, Y. J., Justice, C. O., Flynn, L. P., Kendall, J. D., Prins, E. M., Giglio, L., Ward, D. E., Menzel, W. P., Setzer, A. W. (1998). Potential global fire monitoring from EOS-MODIS. *Journal of Geophysical Research-Atmospheres*, 103(D24), 32215-32238.

Key, C. H., Benson, N. C. (2006). *Landscape Assessment: Ground Measure of Severity, the Composite Burn Index; and Remote Sensing of Severity, the Normalized Burn Ratio*. USDA Forest Service, Rocky Mountain Research Station: Ogden, UT, USA.

Laneve, G., Biase, V. Di (2018). Geostationary Sensor Based Forest Fire Detection and Monitoring: An Improved Version of the SFIDE Algorithm, *Remote Sensing*, 10 (5), 741 p.

Laneve, G., Castronuovo, M.M., Cadau, E.G. (2006). Continuous monitoring of forest fires in the Mediterranean area using MSG. *IEEE Transactions on Geoscience and Remote Sensing*, 44(10), 2761-2768.

Laneve, G., Pampanoni, V., Shaik, R. U. (2020). The Daily Fire Hazard Index: A Fire Danger Rating Method for Mediterranean Areas, *Remote Sens.*, 12, 2356 p. DOI: https://doi.org/10.3390/rs12152356

López García, M. J., Caselles, V. (1991). Mapping burns and natural reforestation using thematic mapper data. *Geocarto Int.*, 6, 31–37.

Li, F., Zhang, X., Kondragunta, S., Roy, D. P. (2017). Investigation of the Fire Radiative Energy Biomass Combustion Coefficient: A Comparison of Polar and Geostationary Satellite Retrievals Over the Conterminous United States, *Journal of Geophysical Research: Biogeosciences*, 123, 722–739. DOI: https://doi.org/10.1002/2017JG004279

Martín, M. P., Ceccato, P., Flasse, S., Downey, I. (1999). *Fire detection and fire growth monitoring using satellite data. Remote sensing of large wildfires*. Springer: Berlin Heidelberg, Germany, 101-122.

Parks, S., Dillon, G., Miller, C. (2014). A New Metric for Quantifying Burn Severity: The Relativized Burn Ratio. *Remote Sensing*, 6(3), 1827–1844. DOI: https://doi.org/10.3390/rs6031827

Prichard, S. J., M. O'Neill, S. M., Eagle, P., Anne G. Andreu, A. G., Drye, B., Dubowy, J., Urbanski S. and Strand, T. M. (2020). Wildland fire emission factors in North America: synthesis of existing data, measurement needs and management applications, *Int. Journal of Wildland Fire*, 29, 132–147.

Prins, E. M., Feltz, J. M., Menzel, W. P., Ward, D. E. (1998). An overview of GOES-8 diurnal fire and smoke results for SCAR-B and 1995 fire season in South America. *Journal of Geophysical Research: Atmospheres*, 103(D24), 31821-31835.

Roberts, G. J., Wooster, M. J. (2008). Fire detection and fire characterization over Africa using Meteosat SEVIRI. *IEEE Transactions on Geoscience and Remote Sensing*, 46(4), 1200-1218.

Robinson, J.M. (1991) Fire from space: Global fire evaluation using infrared remote sensing. *International Journal of Remote Sensing*, 12(1), 3-24.

San-Miguel-Ayanz, J., Durrant, T., Boca, R., Libertà, G. *et al.* (2018). *Forest Fires in Europe*. Publications Office of the European Union; EUR 24910 EN.

Wooster, M. J., Roberts, G., Perry, G. L. W., Kaufman, Y. J. (2005). Retrieval of biomass combustion rates and totals from fire radiative power observations: FRP derivation and calibration relationships between biomass consumption and fire radiative energy release. *Journal of Geophysical Research: Atmospheres*, 110(D24).

Xu, W., Wooster, M. J., Roberts, G., Freeborn, P. (2010). New GOES imager algorithms for cloud and active fire detection and fire radiative power assessment across North South and Central America. *Remote Sensing of Environment*, 114, 1876-1895.

Yi, K., Bao, Y. (2016). Estimates of Wildfire Emissions in Boreal Forests of China, *Forests*, 7(8), 158.